Maderas-Cienc Tecnol 25(2023):27, 1-31
Ahead of Print: Accepted Authors Version

DOI:10.4067/S0718-221X2023005XXXXXX

EVALUATION OF THE INTERFACE OF EUCALYPTUS SPECIMENS WELDED BY ROTARY FRICTION

Ana Carolina Costa Viana [a*]

https://orcid.org/0000-0001-9411-4591

Poliana Dias de Moraes [a]

https://orcid.org/0000-0002-0569-6209

Walter Lindolfo Weingaertner [b]

https://orcid.org/0000-0001-8707-2776

[a]Universidade Federal de Santa Catarina - UFSC, Department of Civil Engineering, Florianópolis, Brazil.
[b]Universidade Federal de Santa Catarina - UFSC, Department of Mechanical Engineering, Florianópolis, Brazil.
***Corresponding author:** anacarolviana@outlook.com
Received: October 25, 2021
Accepted: March 20, 2023
Posted online: March 21, 2023

ABSTRACT

Rotary friction welding produces joints by inserting wood dowels, with a specific rotation and feed rate, into pre-drilled holes made in wood substrates. Studies on the welding of fast-growing eucalypts from Brazilian planted forests are recent. Therefore, this research aimed to evaluate the macro and microstructural and thermochemical changes at the dowel/substrate interface of eucalypts welded joints from Brazilian planted forests and to determine the mechanical strength of two-piece eucalypts welded joints. Specimens formed by eucalypts dowels and substrates were produced. Subsequently, visual evaluation and scanning electron microscopy, attenuated total reflectance-Fourier transform infrared spectroscopy, X-ray diffraction, thermogravimetric, differential scanning calorimetry and tensile tests were performed. The results reveal that the rotary friction welding parameters adopted contribute to the densification of the welded interface and the formation of a structure responsible for joining the dowel and the substrate, providing mechanical strength to the joint. The cellulose crystallinity index and the apparent crystallite size of the eucalypts welded sample increase due to thermal degradation of amorphous components. The rupture of the welded joints is ductile and their average strength is 2,1 MPa. Welded joints of fast-growing eucalypts, from Brazilian planted forests, are suitable when the rotary friction welding parameters are similar to those used for eucalypts woods from Australian forests.

Keywords: Dowel connections, eucalypts wood, rotary friction, thermochemical changes, welding of wood.

INTRODUCTION

Rotary friction welding (RFW) of wood is a recent technique for joining elements from the insertion of dowels, with specific rotation and feed rate, into pre-drilled holes machined in wood substrates. This process causes heating at the interface of the wood pieces in contact, reaching maximum temperatures of 301 °C to 388 °C for rotations between 1000 rpm to 2500 rpm (Rodriguez 2010, Belleville 2012). Consequently, the fusion of polymers occurs in this region, forming an amorphous and dense material, fused with fragments of densified wood fibers (Pizzi *et al.* 2004, Leban *et al.* 2005, Pizzi 2010).

According to Pizzi *et al.* (2004) and Pizzi (2010), the RFW technique has considerable interest, since it is simple, fast, environmentally friendly, more sustainable and low-cost, when compared to adhesives and metal fasteners joint techniques. In addition, RFW joints have mechanical strength comparable to or even higher than glued joints (Pizzi *et al.* 2004). This technique has potential for application in furniture and joinery manufacturing and in engineered wood products, such as dowel-laminated timber (DLT) and dowelled cross-laminated timber (DCLT), used as construction and building materials, alternatively to concrete and steel (Pizzi 2010, Sotayo *et al*. 2020).

According to Belleville *et al*. (2018), eucalypts Australian hardwood is suitable for RFW, since its greater lignin content is favorable to condensation reactions during the RFW process and this is necessary to obtain an effective welded joint. The main *Eucalyptus* species welded by rotary friction are: *saligna* (784 kg/m^3), *pilularis* (925 kg/m^3) and *maculata* (965 kg/m^3) (Belleville *et al.* 2016). The RFW parameters are 1,11 or 1,25 for the dowel/pre-drilled hole diameter ratio and 1230 rpm or 1415 rpm for the rotation (Belleville *et al*. 2016, Belleville *et al*. 2018).

Eucalyptus species from Brazilian planted forests have a higher proportion of sapwood due to their fast growth, caused by favorable edaphoclimatic conditions (Magalhães *et al.* 2012). Mansouri *et al.* (2011) found that the weld line is wider for sapwood than heartwood, since the greater permeability of sapwood allows greater movement of the molten material at the dowel/substrate interface during the welding process. Therefore, differences in wood anatomy influence the quality of welded joints, as well as the chemical composition and structure of wood polymers, mainly lignin and hemicelluloses (Rodriguez 2010).

In Brazil, eucalypts plantations represent 78 % of the total tree planted area (IBÁ 2021). Its wood is commonly used in construction and in furniture and joinery manufacturing (IPT 2022). Few studies have investigated the potential application of the RFW technique to eucalypts woods from Brazilian planted forests. Schneid and Moraes (2016) welded *E. saligna*, with 690 kg/m^3 (IPT 2022), and *Eucalyptus* spp. (794 kg/m^3) using 1,25 for the dowel/pre-drilled hole diameter ratio and 1750 rpm for the rotation. This study found promising results. However, it was focused only on determining the joint strength. Therefore, further research might evaluate the thermochemical changes that occur at the welding interface of these eucalypts woods.

The aim of this research is to evaluate the macro and microstructural and thermochemical changes at the dowel/substrate interface of eucalyptus welded joints from Brazilian planted forests and to determine the mechanical strength of two-piece eucalypts welded joints. Therefore, visual evaluation and scanning electron microscopy (SEM), attenuated total reflectance-Fourier transform infrared spectroscopy (ATR-FTIR), X-ray diffraction (XRD), thermogravimetric (TG), differential scanning calorimetry (DSC) and tensile tests were performed.

MATERIALS AND METHODS

Wood

Eucalyptus hardwood, from planted forests in the state of Paraná - Brazil, was obtained from a sawmill. It has an average apparent density of 938 kg/m^3 ± 12 kg/m^3 at 12 % moisture content (MC).

Samples and specimens (1st phase)

This research was organized into two phases. The 1st phase consisted of macro and microstructural and thermochemical evaluation of the dowel/substrate interface. The sample was composed of 5 specimens formed by the substrate and the dowel, both eucalypts wood. They were produced using smooth dowels (10 mm in diameter and 80 mm in length) and planed rafter as substrate (240 mm × 48 mm × 45 mm), in which five holes of 8 mm in diameter were drilled in the radial-tangential plane of the wood, perpendicularly to the fibers and tangentially to the growth rings (Figure 1). Therefore, the dowel/pre-drilled hole diameter ratio of 1,25 were adopted (Belleville *et al.* 2016, Schneid and Moraes 2016).

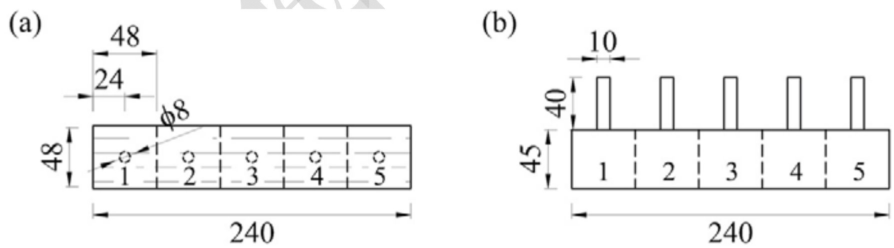

Figure 1: Schematic representation of 1st phase sample (dimensions in mm) (a) top view; (b) front view.

The RFW process consisted of inserting the dowels into the pre-drilled holes machined in the substrates to a depth of 40 mm, using a Charles MVC 955 machining center. The dowel rotation and feed rate were 1000 rpm and 500 mm/min (Viana *et al.* 2021), respectively, resulting in a welding time of 5 s.

After the RFW process, the sample was split into five specimens maintaining the dowels centered in the top position (Figure 1). Subsequently, they were exposed to the ambient temperature and humidity of the laboratory environment for 15 days, to recover the MC lost during the RFW process. Following the stabilization period, samples were taken from the specimens, exposing the welded interface and the unwelded wood, which is named the reference wood in this paper.

Specimens for macrostructural analysis

Three wood specimens measuring 48 mm × 24 mm × 45 mm were used for the macrostructural analysis. They were obtained from a cut perpendicular to the fibers and tangential to the growth rings, as illustrated in Figure 2.

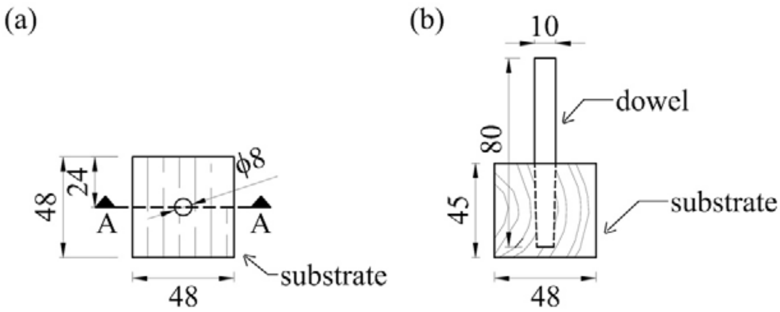

Figure 2: Specimens for visual evaluation (dimensions in mm) (a) top view; (b) front view cut A-A.

Specimens for microstructural analysis

Three wood specimens measuring 15 mm × 10 mm × 5 mm were used for the microstructural analysis (Figure 3). They contained part of the dowel, the welded interface, and the substrate, which were extracted from three specimens of 48 mm × 24 mm × 45 mm. The first specimen (1S) was obtained from a cut perpendicular to the fibers and tangential to the growth rings (Figure 3a), while the second (2S) and the third (3S) specimens were obtained from a cut parallel to the fibers in the tangential and the radial directions to the growth rings, respectively (figures 3b and 3c).

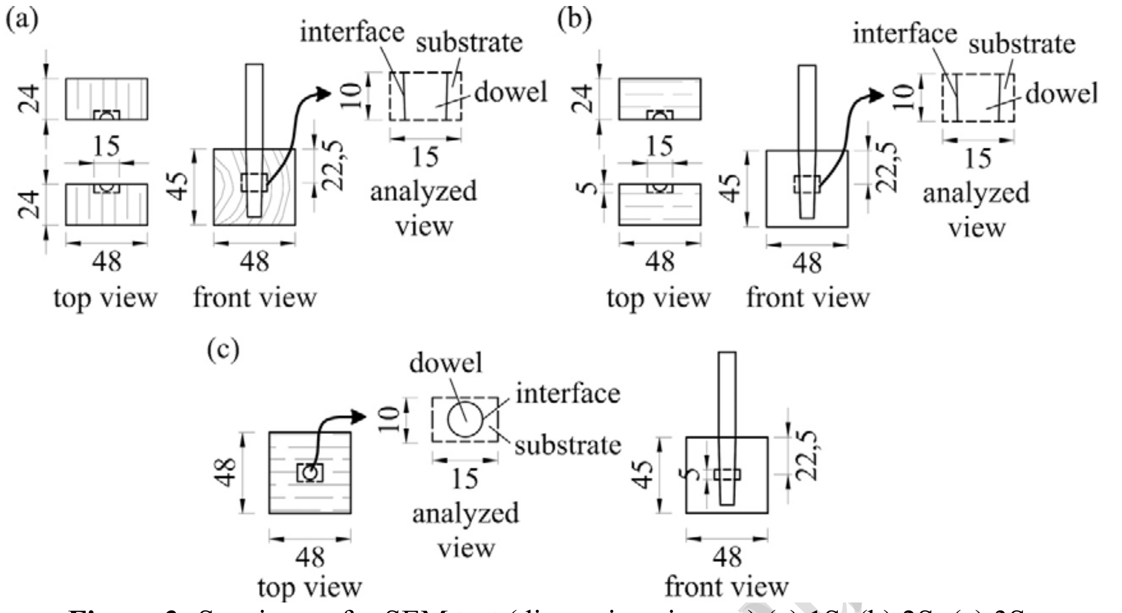

Figure 3: Specimens for SEM test (dimensions in mm) (a) 1S; (b) 2S; (c) 3S.

Samples and specimens for thermochemical analysis

The reference and welded interface specimens, measuring approximately 15 mm × 10 mm × 1 mm, were used for the ATR-FTIR test. The reference and welded interface powdered samples, obtained by scrapping the surface of the specimens, were used for the XRD (100 mg), TG (10 mg) and DSC (5 mg) tests.

Samples and specimens (2nd phase)

The 2nd phase consisted in determining the mechanical strength of two-piece eucalyptus joints. The sample were composed of 5 specimens (1M-5M) formed by the substrate (944 kg/m³ ± 74 kg/m³) and the dowel (861 kg/m³ ± 67 kg/m³), both eucalyptus wood. They were produced using smooth dowels (10 mm in diameter and 80 mm in length) and two-piece substrates (63,5 mm × 50 mm × 50 mm), whose dimensions were based on ABNT NBR 7190 (1997) standard for transverse tensile testing, equivalent to ASTM D143 (2021) standard (Figure 4).

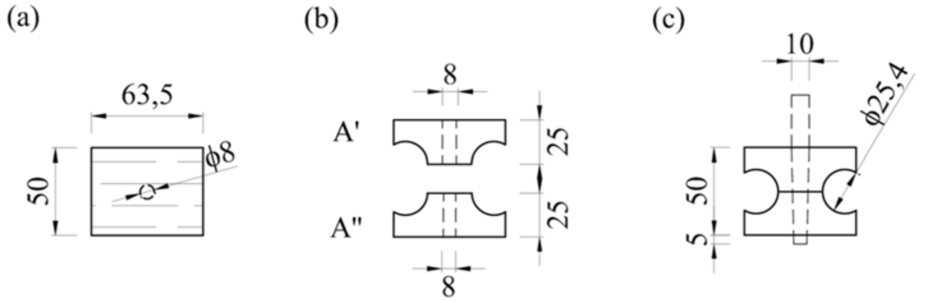

Figure 4: Schematic representation of 2nd phase specimen (dimensions in mm) (a) top view; (b) front view before RFW; (c) front view after RFW.

The dowels and substrates were conditioned at 20 °C ± 2 °C and 60 % ± 5 % relative humidity (RH) (ISO 13061–17 2017) before the RFW process, to maintain 12 % MC. Holes of 8 mm diameter were machined in the radial-tangential plane of the substrates, perpendicularly to the fibers and tangentially to the growth rings. Subsequently, the dowels were welded by rotary friction into the pre-drilled holes, to a depth of 55 mm. The RFW parameters were the same adopted in the 1st phase, resulting in a welding time of 7 s. Later, the specimens were conditioned at the same temperature and RH for 7 days for MC recovery.

Macrostructural analysis

The macrostructural analysis of 1st phase specimens consisted of evaluating the RFW process, the arrangement of substrate growth rings, the color of the welded interface and the dowel and pre-drilled hole shapes resulting from the RFW process.

Tapered dowel measurements

The taper rate of the dowels was determined from the largest and smallest diameters of the dowel, measured using a caliper with an accuracy of 0,01 mm. It is expressed by Eq. 1 (Smid 2003).

$$X = \frac{D - d}{L} \cdot 100, \quad (1)$$

where X is the dowel taper rate, in %; D and d are the largest and the smallest diameters of the dowel, in mm, respectively, and L is the insertion depth of the dowel, in mm.

Microstructural analysis

The microstructural analysis consisted of capturing images of the welded interface using a JEOL JSM-6390LV scanning electron microscope, with an accelerating voltage between 0,5 kV and 30 kV. The specimens were dried in an oven at 40 °C to remove residual moisture, which could influence the quality of the SEM micrographs. Subsequently, they were fixed in stubs, coated with gold in a sputtering system, placed in a sample holder, and then placed in the SEM.

Thermochemical analysis

ATR-FTIR

For the ATR-FTIR analysis, the specimens were placed directly on the crystal of an Agilent Cary 660 FTIR spectrometer, with an ATR accessory (ZnSe crystal). The spectra were obtained at a range of wavenumbers between 4000 cm^{-1} and 650 cm^{-1}, with a resolution of 4 cm^{-1}, recording an average of 32 sweeps. The spectra were normalized from 0 to 1 (Faix 1991).

XRD

For the XRD analysis, the samples were placed in a silicon zero background crystal sample holders, which were prepared by front pressing using a glass slide. Subsequently, they were placed in an X'Pert Pro X-ray diffractometer (PANalytical) PW3040/60. The equipment operated at 45 kV and 40 mA, with CuKa radiation and a wavelength of 1,5418 Å. XRD measurements were recorded by an X'Celerator detector equipped with a graphite monochromator in a scanning range of 5º - 55º (2θ) and a step size of 0,042º (2θ). A knife was used to reduce low-angle air scattering.

The empirical cellulose crystallinity index (CI) was determined by the most commonly used methodology in literature, the Segal method (Segal *et al.* 1959). After baseline subtraction, it was calculated by Eq. 2. In addition, the apparent crystallite size (L) was calculated using Scherrer equation (Eq. 3) (Navi and Sandberg 2011).

$$CI = \frac{I_{200} - I_{am}}{I_{200}} \cdot 100, \quad (2)$$

where CI is the cellulose crystallinity index (%), I_{200} is the maximum intensity of the 200 lattice diffraction and I_{am} is the intensity of the amorphous band (2θ = 18º).

$$L = \frac{0,9 \cdot \lambda}{\beta \cdot \cos\theta}, \quad (3)$$

where L is the apparent crystallite size (nm), λ is the X-ray wavelength (0,15418 nm), β is the half-height width of the diffraction band and θ is the Bragg angle corresponding to the (200) plane.

TG

For the TG analysis, the samples were placed in alumina capsules and then in a NETZSCH STA 449-F3 Jupiter thermal analyzer, where they were heated in a nitrogen atmosphere at a flow rate of 60 ml/min and temperature rate of 10 °C/min, from 23 ºC to 800 ºC.

DSC

For the DSC analysis, the samples were placed in alumina capsules and then in a Jade-DSC Perkin Elmer differential scanning calorimeter, where they were heated in a nitrogen atmosphere at a flow rate of 50 ml/min and temperature rate of 10 °C/min, from 20 ºC to 400 ºC.

Mechanical tensile tests

For the mechanical analysis, the specimens were placed in an Instron 5569 universal testing machine, in which they were subjected to a tensile force parallel to the dowel wood fibers and perpendicular to the substrate wood fibers. The applied load increased monotonically, due to the crossbar displacement at a rate of 2 mm/min, until the joint rupture. Later, the shear engaged by tensile pullout of the dowel was determined from the ratio between the maximum force verified in the tensile test and the welded interface area of piece A”, where the joint breaks. It is expressed by Equation 3 (Viana *et al.* 2022b).

$$\tau = \frac{F_{max}}{\pi \cdot d \cdot h}, \qquad (3)$$

where τ is the shear stress, in MPa; F_{max} is the maximum force, in N; *d* is the pre-drilled hole diameter (8 mm); *h* is the piece A" height, in mm.

RESULTS AND DISCUSSIONS

Macrostructural analysis

During the RFW process, some events were observed: the smoke emissions, which are, according to Omrani *et al.* (2008), water vapour, CO_2 and degradation compounds from carbohydrates, mainly hemicelluloses, and lignin (Figure 5); the darkening of the welded interface; and the wear of the dowel and the pre-drilled hole. As stated in Yin *et al.* (2022), these events are due to the contact pressure between the dowel and the pre-hole surfaces and the high temperatures reached during this process, which intensity depends on the RFW parameters adopted and the welding time.

The cross-sections of a specimen, before and after the extraction of the dowel, are illustrated in Figure 6. During the dowel insertion in the substrate, it passed through regions with distinct anatomical and physical characteristics (Figure 6a), since the arrangement of the growth rings in the cross-section is not symmetrical to the pre-hole axis.

Figure 5: Welding process.

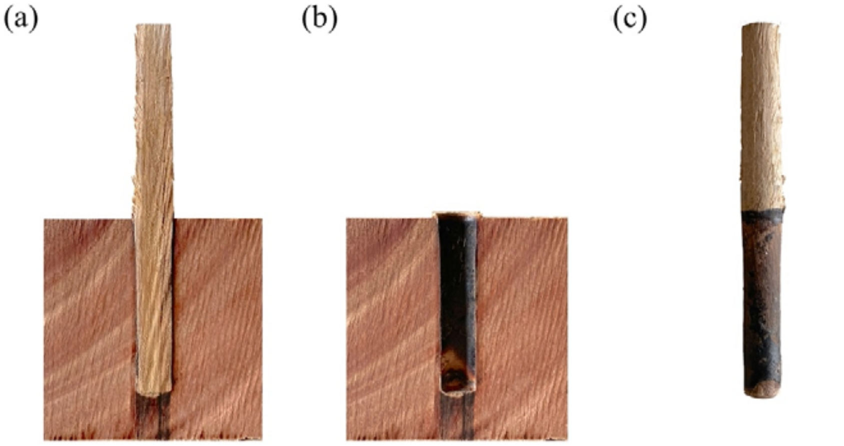

Figure 6: Sectioned specimen after RFW (a) dowel and substrate; (b) substrate; (c) dowel.

The darkening of the dowel/substrate interface (Figure 6b) is due to hydrolysis of hemicelluloses, reactions of sugars with amino acids and condensation and oxidation of lignin phenolic compounds (Peña 2018). The pre-drilled hole and the dowel, originally cylindrical, assume a conical shape due to their wear (Figure 6c). As the dowel is inserted into the pre-drilled hole, its diameter reduces gradually, while the pre-drilled hole diameter increases. Thus, the dowels had an average taper rate of 4,2 % and a standard deviation of 0,1 %.

Microstructural analysis

The scanning electron micrographs of 1S, 2S and 3S specimens are illustrated in Figure 7. The micrographs show that the RFW of eucalyptus wood reproduces the behavior described in the literature for other wood species, even had a higher average apparent density (938 kg/m^3 ± 12 kg/m^3). There is a space between the dowel/substrate interface (figures 7a and 7b), as reported by Properzi *et al.* (2005) when welding *Fagus sylvatica* hardwood (450 kg/m^3 - 600 kg/m^3). Figure 6c shows an intercellular material adhered to the substrate interface, which is composed mainly of lignin present in the middle lamella of the wood, keeping the cells interconnected, as reported by Gfeller *et al.* (2003) when welding *F. sylvatica*.

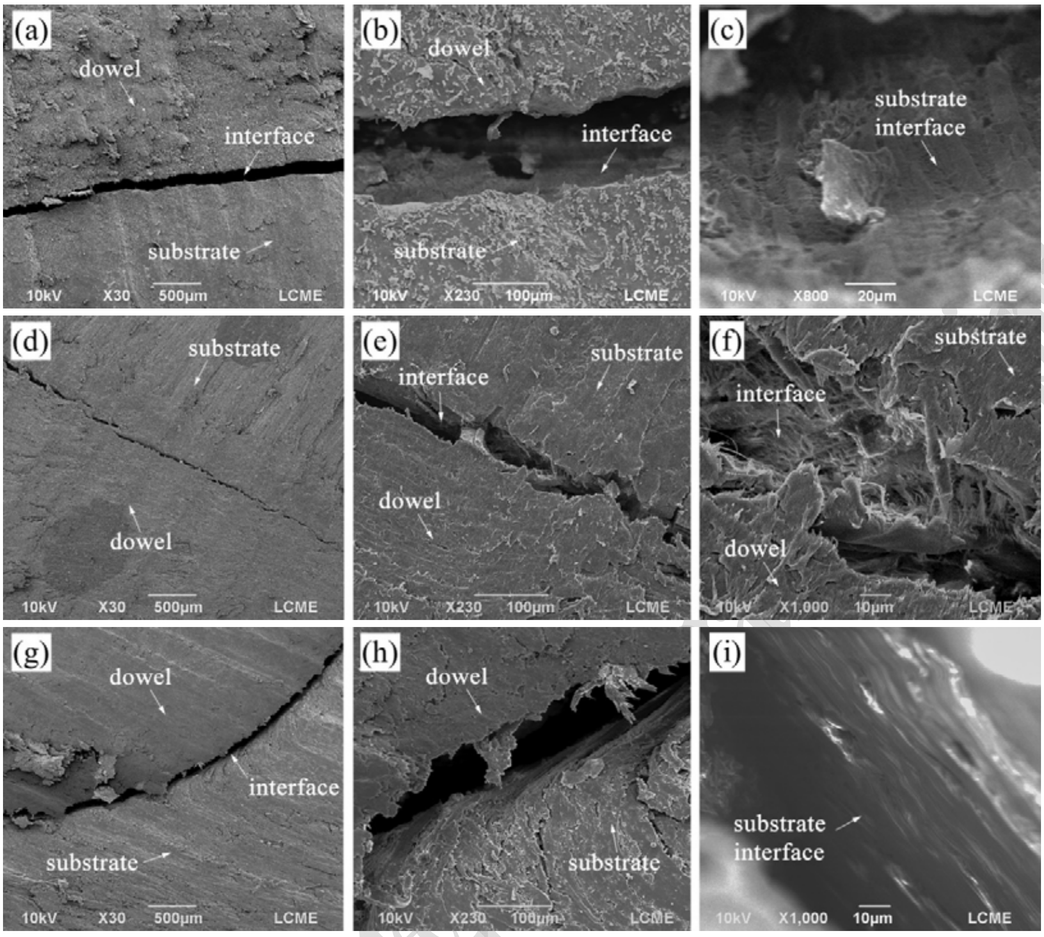

Figure 7: Scanning electron micrographs of welded interfaces (a-c) 1S specimen; (d-f) 2S specimen; (g-i) 3S specimen.

For the RFW parameters adopted, the wood fibers intertwined at the interface and formed a microstructure responsible for joining the dowel and the substrate, providing mechanical strength to the joint (Zhu *et al.* 2017b) (figures 7d-f). Hongda *et al.* (2022) reported a similar behavior when welding *Phyllostachys edulis* (680 kg/m^3) bamboo dowels in European spruce (700 kg/m^3) substrates, with feed rates of 200 mm/min, 600 mm/min and 800 mm/min.

The fibers at the edge of the substrate interface flowed in the direction of rotational movement, due to the forced insertion of the dowel and the consequent increase in temperature (figures 7g-h) (Pizzi *et al.* 2004). Figure 7i illustrates the deformation and the densification of wood cells at the substrate interface due to the contact pressure and the heating induced by the RFW process. According to Leban *et al.* (2004), this contributes to the welded joint strength.

Thermochemical analysis

ATR-FTIR

The ATR-FTIR spectra of reference and welded wood specimens are illustrated in Figure 8. The shape of the spectra is similar to those obtained by Belleville *et al.* (2018) when welding Australian *E. saligna* and *E. pilularis* with a rotation of 1230 rpm and a dowel/pre-drilled hole diameter ratio of 1,26. These parameters are similar to those adopted in this research.

The main changes resulting from the RFW process are verified in the 3600 cm^{-1} - 2800 cm^{-1} and 1500 cm^{-1} - 850 cm^{-1} bands. The 3600 cm^{-1} - 3100 cm^{-1} band corresponds to the stretching of hydroxyl groups (O-H) (Delmotte *et al.* 2008). The low peak at 3336 cm^{-1}, for the welded specimen, is due to dehydration reactions, caused by water loss during the RFW process (Kanazawa *et al.* 2005, Esteves *et al.* 2013). This change increases dimensional stability by reducing hygroscopicity and water absorption at the wood-welded interface (Amirou *et al.* 2019).

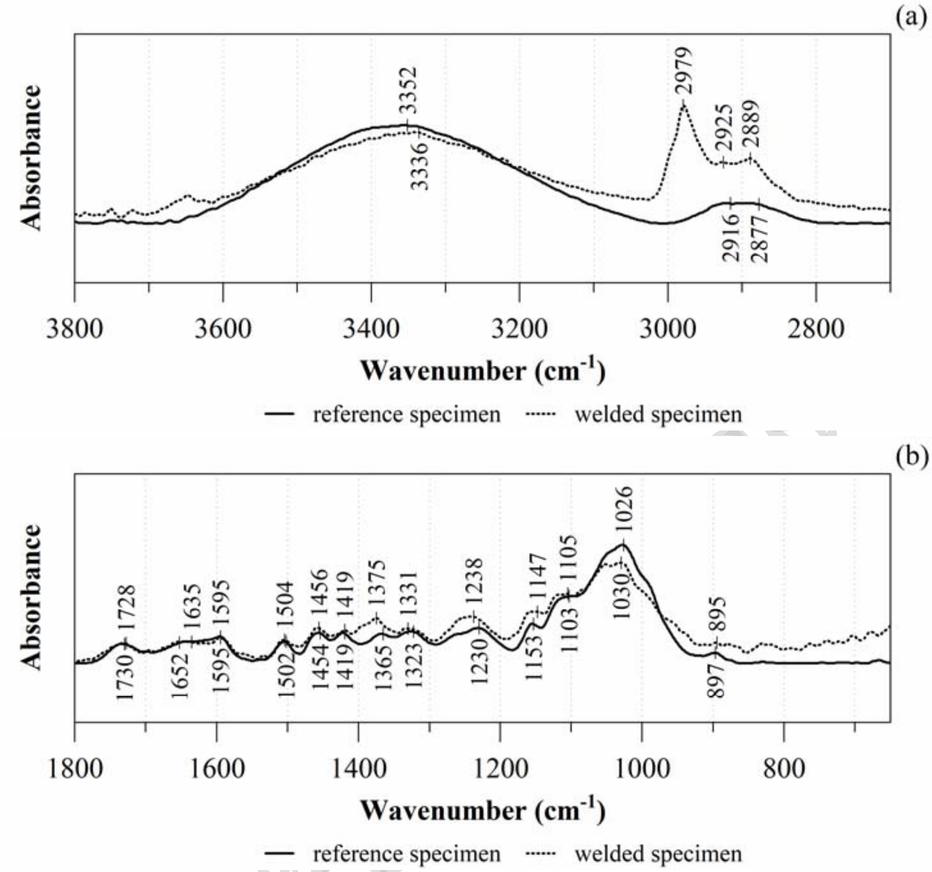

Figure 8: ATR-FTIR spectra of the reference and welded specimens (a) 3800 cm^{-1} - 2700 cm^{-1} band; (b) 1800 cm^{-1} - 650 cm^{-1} band.

The 3000 cm^{-1} - 2800 cm^{-1} band is attributed to the stretching of methyl (CH_3) and methylene (CH_2) groups (Esteves *et al.* 2013, Dias Jr. *et al.* 2017). The high peaks at 2979 cm^{-1}, 2925 cm^{-1} and 2889 cm^{-1}, for the welded specimen, is due to changes in cellulose crystallinity and lignin (Dias Jr. *et al.* 2017).

The 1456 cm^{-1} - 1419 cm^{-1} band corresponds to asymmetric C-H deformations in lignin and C-H bending in cellulose (Özgenc *et al. 2*017, Kubovský *et al.* 2020). It is higher for the welded specimen due to lignin alteration resulting from condensation and/or formation of CH_2 bridges between lignin fragments and the increase in the amount of crystalline cellulose

(Belleville 2012, Kubovský *et al.* 2020). Li *et al.* (2021) observed the increase of a nearby peak (1462 cm^{-1}) when welding *Phyllostachys pubescens* (680 kg/m³) bamboo dowels in *Populus* sp. (450 kg/m³) substrates, using a rotation of 1500 rpm and a feed rate of 400 mm/min - 450 mm/min. The feed rate is similar to that used in this research (500 mm/min).

The 1380 cm^{-1} - 1300 cm^{-1} band is assigned to C-H bending in cellulose and hemicelluloses (Kubovský *et al.* 2020). For the welded specimen, the 1375 cm^{-1} and 1331 cm^{-1} peaks are higher due to the increase of condensed structures (Esteves *et al.* 2013; Kubovský *et al.* 2020). In addition, the 1331 cm^{-1} - 1323 cm^{-1} band indicates the splitting of ether bonds from lignin (Belleville *et al.* 2013).

The peaks at 1300 cm^{-1} - 1200 cm^{-1} and 950 cm^{-1} - 850 cm^{-1} bands are more intense for the welded specimen due to acetyl group splitting from hemicelluloses, causing the production of acid substances in the welded interface, as reported by Belleville (2012) when welding *Acer saccharum* and *Betula alleghaniensis* hardwoods with a rotation of 1230 rpm.

The 1200 cm^{-1} - 1000 cm^{-1} band is assigned to C-O-C stretching in cellulose, hemicelluloses and lignin (Kubovský *et al.* 2020). For the welded specimen, the 1147 cm^{-1} and 1105 cm^{-1} peaks are higher and the 1030 cm^{-1} peak are lower, when compared to the reference specimen. The first behavior suggests dehydration reactions forming covalent intermolecular bonds and the latter indicates the beginning of cellulose degradation processes and the partial demethoxylation of lignin and its gradual crosslinking (Kubovský *et al.* 2020).

XRD

The XRD patterns of the reference and welded wood samples are illustrated in Figure 9. The X-ray diffractograms are similar to those obtained by Zhu *et al.* (2017b) and by Zor *et al.* (2021), when welding *B. pendula*, *L. Gmelinii, Abies bornmulleriana*, *Quercus robur* and

Castanea sativa from northern hemisphere. These patterns refer to cellulose Iβ (JINROO01-CSD), whose main peaks are 14,9º, 16,6º, 22,9º and 34,4º (2θ) (Groom *et al.* 2016).

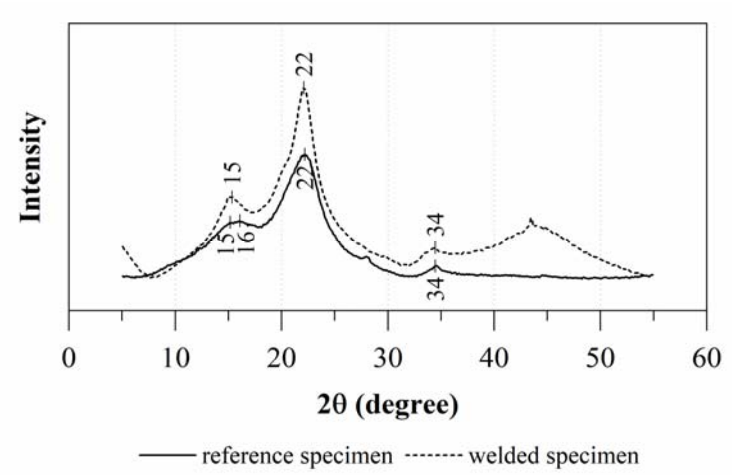

Figure 9: X-ray diffractograms of the reference and welded samples.

The peaks are more pronounced for the welded sample. It indicates that there were changes in the cellulose crystallinity, as observed in the ATR-FTIR spectra (Figure 8). This is also confirmed by the cellulose CI which corresponds to 65 % and 59 % for the welded and reference samples, respectively. Zhu *et al.* (2017b) reported a similar behavior when welding *B. pendula* dowels in *L. gmelinii* substrates using a rotation of 1080 rpm and feed rate of 600 mm/min, parameters similar to those adopted in this research.

The apparent crystallite size (L) is 2,9 nm and 2,4 nm for the welded and reference samples, respectively. The greater L and cellulose CI for the welded sample suggests that the proportion of crystalline cellulose increased due to the RFW process. The contact pressure and the high temperatures cause the hydrolysis of polysaccharides, the production of acid substances from acetyl groups of hemicelluloses and the splitting of ether bonds from lignin, as verified in the ATR-FTIR spectra (Figure 8). Consequently, a reduction in the amorphous phase from the sample, since the polymers become more mobile, leaving cellulose free to fuse and form larger diameter fibrils and microfibrils (Navi and Sandberg 2011). According to Navi and Sandberg (2011), the greater L and cellulose CI, together with interface densification observed in the SEM micrographs, contributes to the stiffness and strength of the joint.

TG

The thermogravimetric behavior of the reference and welded wood samples and their first derivatives (DTG) are illustrated in Figure 10. The thermal degradation process is divided into three phases: dehydration, at a range from 20 ºC to 200 ºC; active pyrolysis, at a range from 200 ºC to 385 ºC; and passive pyrolysis after 385 ºC (Slopiecka *et al.* 2012). At the initial heating temperatures, the DTG behavior of the samples shows a relative minimum due to the evaporation of water and volatile wood extractives (Slopiecka *et al.* 2012, Zhu *et al.* 2017b). This occurs at 90 ºC for the reference and welded samples, with a mass loss of 6,2 % and 5,8 %, respectively. The mass loss of the welded sample is 0,4 % lower, since the high temperatures reached in the RFW process reduce the number of accessible OH groups, as found in the ATR-FTIR test (Figure 8). Similar behavior was obtained by Zhang *et al.* (2018) when welding *Betula* spp. dowels in *L. gmelinii* substrates, with welding times of 3 s, 5 s and 7 s and rotation of 2400 rpm. The welding times are similar to those of this research, however, the rotation is much higher.

The DTG behavior shows a relative maximum at 153 ºC, for the reference sample, and, at 150 ºC, for the welded sample. According to Crespo *et al.* (2015), these maximum points are due to the complete evaporation of water and volatile extractives. As the temperature increases, the chemical bonds are broken due to dehydration reactions (Rowell 2005). At 290 ºC, the DTG of the reference sample shows a slope change characterized by the pyrolysis of hemicelluloses (Rowell 2005). It is caused by the deacetylation and by the release of acetic acid and formic acid (Navi and Sandberg 2011, Poletto *et al.* 2012a), which was observed in the 1238 cm^{-1} - 1230 cm^{-1} and 897 cm^{-1} - 895 cm^{-1} bands of the ATR-FTIR spectra (Figure 8). The DTG of the welded sample does not show a slope change, since part of hemicelluloses was decomposed during RFW (Stamm *et al.* 2006). According to Poletto *et al.* (2012b), the susceptibility of hemicelluloses to thermal decomposition can be attributed to its random amorphous structure, which is easily hydrolyzed. Zhu *et al.* (2017a) reported similar temperatures for the pyrolysis of hemicelluloses, between 227 ºC and 327 ºC, when welding *Betula* spp. and *L. gmelinii* woods, with a rotation of 1000 rpm. The same rotation used in this research.

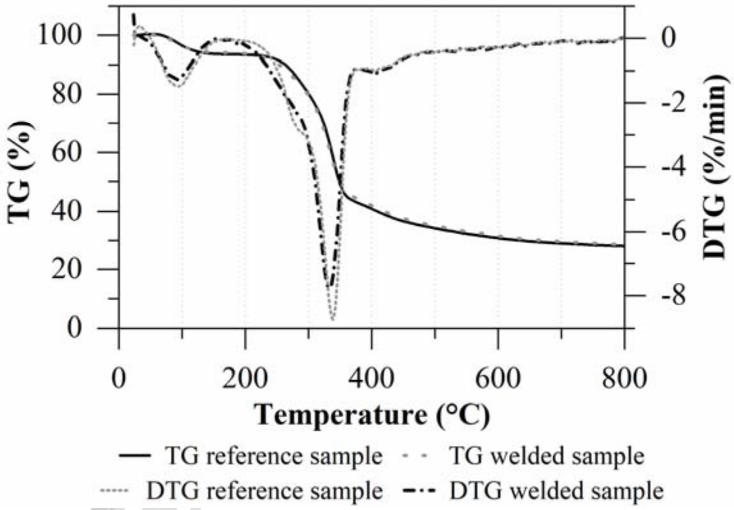

Figure 10: TG/DTG thermograms of the reference and welded samples.

The DTG behavior shows a relative minimum around 335 ºC due to the pyrolysis of cellulose, which is less intense for the welded sample. This is probably caused by chemical changes in the amorphous regions of microfibrils during the RFW process (Sun *et al.* 2010). At 348 ºC, the reference and welded samples lost 50 % of their mass. Belleville *et al.* (2018) obtained similar results when welding *E. pilularis* (345 ºC).

Between 350 ºC and 800 ºC, the samples show a continuous and slow mass loss due to lignin pyrolysis, which occurs in a wide temperature range (Crespo *et al.* 2015). This results in a more condensed structure, as verified in the ATR-FTIR test, which contributes to the mechanical strength of the welded joint (Sun *et al.* 2010). In this temperature range, the mass loss is less pronounced for the welded sample, since the chemical reactions during RFW increase the complexity and the thermal stability of polymers at the welded interface (Belleville *et al.* 2018).

The extractives, mainly volatiles, degrade between 150 ºC and 600 ºC, causing the emergence of new extractable compounds, resulting from the thermal decomposition of cell wall structural components of the wood (Esteves and Pereira 2009; Zhu *et al.* 2018).

DSC

The thermograms, represented in Figure 11, illustrate the DSC behavior of the reference and welded wood samples. The relative maximum (endothermic) peaks, between 20 ºC - 125 ºC, 160 ºC - 285 ºC and 300 ºC - 375 ºC, are due to volatilization and tar formation processes (Strezov *et al.* 2003, Ball *et al.* 2004). Between 125 ºC - 160 ºC, 285 ºC - 300 ºC and after 375 ºC, the relative minimums (exothermic) are derived from the decomposition and carbonization of wood compounds (Strezov *et al.* 2003, Ball *et al.* 2004).

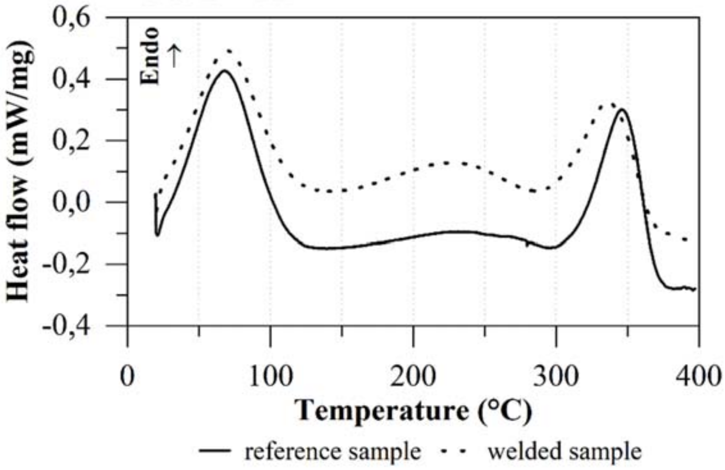

Figure 11: DSC thermograms of the reference and welded samples.

In general, the temperature and the intensity of the relative maximum and minimum are lower for the welded sample than the reference sample. This behavior indicates that the RFW process causes changes in the chemical composition of the welded interface, as noticed by the XRD results (cellulose crystallinity). Sun *et al.* (2010) also reported a reduction in the intensity of relative maximum (exothermic) peaks when welding *B. alleghaniensis* hardwood.

The first relative maximum (endothermic) peak, at 68 ºC, for the reference sample, and, at 70 ºC, for the welded sample, is due to the water evaporation (Strezov *et al.* 2003, Poletto 2016). The heat flow intensity for the welded sample is 9 % lower than that of the reference sample. This lower intensity is due to the loss of OH groups caused by high temperatures reached during the RFW process. Pereira (2017) also verified the reduction in intensity of the endothermic peak between 50 ºC and 100 ºC, after heating *E. urophylla* wood, up to 260 ºC.

As the temperature increases, the wood polymers soften, mainly hemicelluloses, which are more susceptible to high temperatures (Vaziri and Sandberg 2021). At 140 ºC, the DSC thermograms show a first relative minimum (exothermic) hump assigned to the complete evaporation of free and adsorbed water present in the wood (Esteves and Pereira 2009).

A secondary relative maximum (endothermic) peak is observed at 231 ºC, for the reference sample, and, at 225 ºC, for the welded sample. It is characterized by the degradation of lignin and, mainly, hemicelluloses, due to their thermal decomposition (Strezov *et al.* 2003, Poletto 2016, Wulfhorst *et al.* 2016). The intensity of the heat flow at this peak is 44 % higher for the welded sample than for the reference sample, since the intercellular material at the welded interface has more lignin condensed structures, as verified in the ATR-FTIR test (Pizzi *et al.* 2006, Stamm *et al.* 2006).

A second relative minimum (exothermic) hump is observed at 294 ºC for the reference sample and, at 286 ºC, for the welded sample. It is attributed to the primary pyrolysis of hemicelluloses and the consequent formation of furfurals and acetic acids (Strezov *et al.* 2003, Yang *et al.* 2007), since hemicelluloses are the least thermally stable and, therefore, more susceptible to thermal degradation caused by RFW (Stamm *et al.* 2006).

Increasing the temperature, a third relative maximum (endothermic) peak is observed at 346 ºC, for the reference sample, and, at 336 ºC, for the welded sample. This peak is due to the pyrolysis of cellulose, caused by depolymerization, decomposition, and volatilization (Lee *et al.* 2003, Yang *et al.* 2007, Wulfhorst *et al.* 2016). Its temperature and intensity reduce after RFW, indicating that part of cellulose, mainly amorphous fraction, is decomposed during the RFW process (Sun 2010, Zhu *et al.* 2017b), as observed in the ATR-FTIR and TG/DTG results. Khalimov *et al.* (2019) reported very similar behavior for birch wood, with 690 kg/m^3 (Meier 2021), when comparing a reference sample and a pyrolyzed wood sample.

The enthalpy of fusion of cellulose corresponds to 18,2 J/g and 15,1 J/g for the reference and welded samples, respectively. The enthalpy value is lower after welding, probably due to the partial degradation of cellulose during RFW of the wood (Zhu *et al.* 2017a). Above 375 ºC, the heat flow of the DSC thermograms starts to decrease due to the condensation reactions (Tsujiyama *et al.* 2000).

Mechanical strength

The load × displacement curves of 1M to 5M specimens are illustrated in Figure 12. An almost linear increase in force is observed, until reaching the maximum load. Subsequently, there is a gradual failure of the joint, characterizing a ductile rupture. Belleville (2012) reported the same behavior for *B. alleghaniensis* dowels welded unidirectionally in two-piece substrates of the same species, which is a hardwood as eucalyptus species.

The welded surface strength of eucalyptus specimens is presented in Table 2. The average strength and the coefficient of variation are 2,1 MPa and 18 %, respectively. The variation in the results may be related to the wood heterogeneity, since Belleville *et al.* (2016) obtained similar coefficients of variation (10 % to 25 %) when welding *E. saligna* and *E. pilularis* by rotary friction, with a rotation of 1000 rpm.

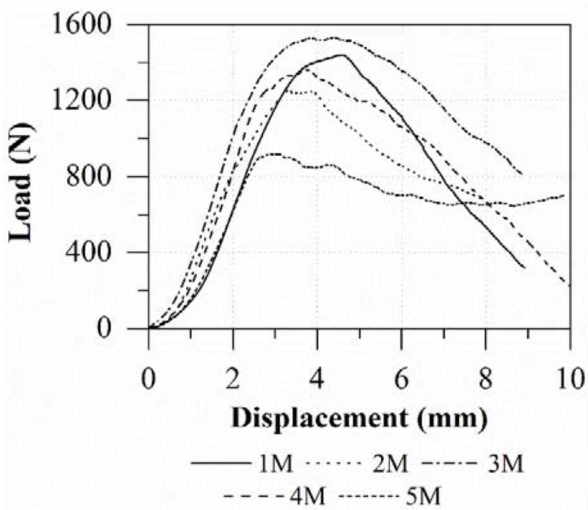

Figure 12: Load × displacement curve.

Table 2: Shear strength of eucalypts specimens.

Specimen	1M	2M	3M	4M	5M	Mean	Standard deviation
Shear strength (MPa)	2,3	2,0	2,4	2,1	1,5	2,1	0,4

Schneid and Moraes (2016) obtained an average strength of 3,0 MPa when welding *E. saligna* dowels (12 mm in diameter) into pre-drilled holes (10 mm in diameter) machined in *Eucalyptus* spp. (794 kg/m³) substrates composed by two pieces, to a depth of 50 mm. The rotation and the feed rate were 1750 rpm and 750 mm/min, respectively. The strength is 30 % greater than that obtained in this research. This may be due to the different adopted RFW parameters.

Viana *et al.* (2022a) reported an average strength of 0,7 MPa when welding *Mezilaurus itauba* (824 kg/m³ ± 8 kg/m³) dowels with 10 mm in diameter into pre-drilled holes, with 8 mm in diameter, machined in *Pinus taeda* (606 kg/m³ ± 10 kg/m³) substrates composed of two pieces, to a depth of 55 mm. The rotation, the feed rate and the dowel/pre-drilled hole were 1000 rpm, 500 mm/min and 1,25, respectively. The strength is 67 % lower than that obtained in this research, probably, due to the different dowel and substrate wood species, since the RFW parameters are the same adopted in this research.

The results obtained in this research demonstrate the potential of fast-growing eucalypts woods, from Brazilian planted forests, to be welded adopting RFW parameters similar to those used for Australian eucalypts and northern hemisphere woods. However, further studies should focus on determining the optimal RFW parameters to obtain the best mechanical performance of the joint.

CONCLUSIONS

In this research, eucalypts RFW joints from Brazilian planted forests were evaluated based on the macro and microstructural, thermochemical and mechanical analyses. The results allow us to conclude that:

- the adopted RFW parameters contribute to the densification of the welded interface and the formation of a structure responsible for joining the dowel and the substrate, providing mechanical strength to the joint;
- the cellulose CI and the apparent crystallite size of the eucalypts welded sample are greater due to thermal degradation of amorphous components;
- the rupture of eucalypts welded joints is ductile and their average strength is 2,1 MPa;

- welded joints of fast-growing eucalypts, from Brazilian planted forests, have suitable strength when the RFW parameters are similar to those used for eucalypts woods from Australian forests.

AUTHORSHIP CONTRIBUTIONS

A. C. C. V.: Conceptualization, data curation, formal analysis, investigation, methodology, writing – original draft, writing – review & editing; P. D. M.: Conceptualization, methodology, project administration, supervision, writing – original draft, writing – review & editing; W. L. W.: Project administration, supervision, writing – review & editing.

ACKNOWLEDGEMENTS

The authors thank the Coordination for the Improvement of Higher Education Personnel (CAPES) (Finance Code 001). The authors acknowledge the staff of Precision Mechanical Laboratory (LMP-UFSC), Central Laboratory of Electronic Microscopy (LCME-UFSC), Process Control Laboratory (LCP-UFSC), Central Analysis EQA (Central de Análises EQA-UFSC), X-ray Diffraction Laboratory (LDRX-UFSC) and Laboratory for Nanotechnology Applications in Civil Construction (NANOTEC-UFSC) for technical support during RFW process and SEM, ATR-FTIR, XRD, TG, DSC and tensile tests.

REFERENCES

Associação Brasileira de Normas Técnicas. ABNT. 1997. Projeto de estruturas de madeira. NBR 7190. ABNT, Rio de Janeiro, Brazil**.**

Amirou, S.; Pizzi, A.; Delmotte, L. 2019. Investigations of mechanical properties and chemical. *J Adhes Sci Technol* 34(1): 13-24. https://doi.org/10.1080/01694243.2019.1659569

American Society for Testing and Materials. ASTM. 2021. Standard test methods for small clear specimens of timbers. ASTM D143. ASTM, West Conshohocken, United States.

Ball, R.; McIntosh, A.C.; Brindley, J. 2004. Feedback processes in cellulose thermal decomposition: implications for fire-retarding strategies and treatments. *Combust Theor Model* 8(2): 281-291. https://doi.org/10.1088/1364-7830/8/2/005

Belleville, B. 2012. Soudage de bois feuillus par friction rotationnelle. Ph.D. Thesis, University of Laval. Québec, Canada. (In French)

Belleville, B.; Stevanovic, T.; Pizzi, A.; Cloutier, A.; Blanchet, P. 2013. Determination of optimal wood-dowel welding parameters for two North American hardwood species. *J Adhes Sci Technol* 27(5-6): 566-576. https://doi.org/10.1080/01694243.2012.687596

Belleville, B.; Ozarska, B.; Pizzi, A. 2016. Assessing the potential of wood welding for Australian eucalypts and tropical species. *Eur J Wood Prod* 74: 753-757. https://doi.org/10.1007/s00107-016-1067-5

Belleville, B.; Koumba-Yoya, G.; Stevanovic, T. 2018. Effect of wood welding process on chemical constituents of Australian Eucalyptus. *J Wood Chem Technol* 39(1): 43-56. https://doi.org/10.1080/02773813.2018.1494745

Crespo, Y.A.; Naranjo, R.A.; Burgos, J.C.V. 2015. Thermogravimetric analysis of thermal and kinetic behavior of *Acacia mangium* wood. *Wood Fiber Sci* 47(4): 327-335. https://wfs.swst.org/index.php/wfs/article/view/2363

Delmotte, L.; Ganne-Chedeville, C.; Leban, J.M.; Pizzi, A.; Pichelin, F. 2008. CP-MAS 13C NMR and FT-IR investigation of the degradation reactions of polymer constituents in wood welding. *Polym Degrad Stab* 93(2): 406-412. https://doi.org/10.1016/j.polymdegradstab.2007.11.020

Dias Jr., A.F.; Oliveira de, R.N.; Deglise, X.; Souza de, N.D.; Brito, J.O. 2019. Infrared spectroscopy analysis on charcoal generated by the pyrolysis of *Corymbia citriodora* wood. *Revista Matéria* 24(3). https://doi.org/10.1590/S1517-707620190003.0700

Esteves, B.M.; Pereira, H.M. 2009. Wood modification by heat treatment: A review. *BioResources* 4(1): 370-404. http://doi.org/10.15376/biores.4.1.370-404

Esteves, B.; Marques, A.V.; Domingos, I.; Pereira, H. 2013. Chemical changes of heat treated pine and eucalypt wood monitored by FTIR. *Maderas-Cienc Tecnol* 15(2): 245-258. http://dx.doi.org/10.4067/S0718-221X2013005000020

Faix, O. 1991. Condensation indices of lignins determined by FTIR-spectroscopy. *Holz Roh Werkst* 49(9): 356.

Gfeller, B.; Zanetti, M.; Properzi, M.; Pizzi, A.; Pichelin, F.; Lehmann, M.; Delmotte, L. 2003. Wood bonding by vibrational welding. *J Adhes Sci Technol* 17(11): 1573-1589. https://doi.org/10.1163/156856103769207419

Groom, C.R.; Bruno, I.J.; Lightfoot, M.P.; Ward, S.C. 2016. The Cambridge structural database. *Acta Crystallogr* 171–179. https://doi.org/10.1107/S2052520616003954

Hongda, Y.; Ning, W.; Xinmiao, M.; Xudong, Z.; Ying, G. 2022. Study on process parameters and mechanism of bamboo dowel rotation welding. *J Beijing For Univ* 44(2): 141-150. 10.12171/j.1000-1522.20210288 (In Chinese)

Indústria Brasileira de Árvores. IBA. 2021. *IBÁ Annual Report*. IBÁ, São Paulo, Brasil. https://www.iba.org/datafiles/publicacoes/relatorios/relatorioiba2021-compactado.pdf

Instituto de Pesquisas Tecnológicas. IPT. 2022. *Informações sobre madeiras*. IPT, São Paulo, Brasil. https://www.ipt.br/informacoes_madeiras/13-eucalipto_grandis.htm (In Portuguese)

ISO. 2017. Physical and mechanical properties of wood - Test methods for small clear wood specimens. ISO 13061–17. International Organization for Standardization, Geneva, Switzerland.

Kanazawa, F.; Pizzi, A.; Properzi, M.; Delmotte, L.; Pichelin, F. 2005. Parameters influencing wood-dowel welding by high-speed rotation. *J Adhes Sci Technol* 19(12): 1025-1038. https://doi.org/10.1163/156856105774382444

Khalimov, E.; Shteba, T.; Yuryev, Y. 2019. Some peculiarities of burnt birch wood pyrolysis. *IOP Conf Ser: Earth Environ Sci* 316. 012019. http://doi.org/10.1088/1755-1315/316/1/012019

Kubovský, I.; Kačíková, D.; Kačík, F. 2020. Structural changes of oak wood main components caused by thermal modification. *Polymers* 12(2): 485. https://doi.org/10.3390/polym12020485

Leban, J.M.; Pizzi, A.; Wieland, S.; Zanetti, M.; Properzi, M.; Pichelin, F. 2004. X-ray microdensitometry analysis of vibration-welded wood. *J Adhes Sci Technol* 18(6): 673-685. https://doi.org/10.1163/156856104839310

Leban, J.M.; Pizzi, A.; Properzi, M.; Pichelin, F.; Gelhaye, P.; Rose, C. 2005. Wood welding: a challenging alternative to conventional wood gluing. *Scand J For Res* 20(6): 534-538. https://doi.org/10.1080/02827580500432305

Lee, H-L.; George, C.C.; Rowell, R.M. 2003. Thermal properties of wood reacted with a phosphorus pentoxide–amine system. *J Appl Polym Sci* 91(4): 2465-2481. https://doi.org/10.1002/app.13408

Li, S.; Zhang, H.; Shu, B.; Cheng, L.; Ju, Z.; Lu, X. 2021. Study on the bonding performance of the moso bamboo dowel welded to a poplar substrate joint by high-speed rotation. *J Renew Mater* 9(7): 1225-1237. http://dx.doi.org/10.32604/jrm.2021.014364

Magalhães, W.L.E.; Mattos, B.D.; Missio, A.L. 2012. Field testing of CCA-treated Brazilian spotted gum. *Int Biodeter Biodegr* 74: 124-128. http://doi.org/10.1016/j.ibiod.2012.05.024

Mansouri, H.R.; Pizzi, A.; Leban, J.M.; Delmotte, L.; Lindgren, O.; Vaziri, M. 2011. Causes for the improved water resistance in pine wood linear welded joints. *J Adhes Sci Technol* 25(16): 1987-1995. https://doi.org/10.1163/016942410X544794

Meier, E. 2021. Loblolly Pine. The wood database. https://www.wood-database.com/loblolly-pine/.

Navi, P.; Sandberg, D. 2011. *Thermo-hydro-mechanical wood processing*. EPFL Press, New York, USA. https://doi.org/10.1201/b10143

Omrani, P.; Masson, E.; Pizzi, A.; Mansouri, H.R. 2008. Emission of gases and degradation volatiles from polymeric wood constituents in friction welding of wood dowels. *Polym Degrad Stab* 93: 794-799. https://doi.org/10.1016/j.polymdegradstab.2008.01.017

Özgenc, Ö.; Durmaz, S.; Boyaci, I.H.; Eksi-Kocak, H. 2017. Determination of chemical changes in heat-treated wood using ATR-FTIR and FT Raman spectrometry. Sp*ectrochim Acta A* 171: 395-400. https://doi.org/10.1016/j.saa.2016.08.026

Peña, M.I.P. 2018. Caractéristiques chimiques et anatomiques de la ligne de soudure du bois. Ph.D. Thesis, Lorraine University. Nancy, France. (In French)

Pereira, M.P.C.F 2017. Decomposição térmica e biológica de cavacos de *Eucalyptus urophylla*. Master, Universidade Federal de Viçosa, Viçosa, Brazil. (In Portuguese) https://www.locus.ufv.br/handle/123456789/11564

Pizzi, A.; Leban, J.M.; Kanazawa, F.; Properzi, M.; Pichelin, F. 2004. Wood dowel bonding by high-speed rotation welding. *J Adhes Sci Technol* 18(11): 1263-1278. https://doi.org/10.1163/1568561041588192

Pizzi, A.; Despres, A.; Mansouri, H.R.; Leban, J.M.; Rigolet, S. 2006. Wood joints by through-dowel rotation welding- microstructure, 13C-NMR and water resistance. *J Adhes Sci Technol* 20(5): 427-436. http:// doi.org/10.1163/156856106777144327

Pizzi, A. 2010. Wood joints adhesion and performance in mechanical friction welding of wood without adhesives. Chapter 9. 8p. In: *Recent advances in adhesion science and technology*. Gutowski, W.; Dodiuk, H. (Eds.). CRC Press, Boca Raton, Florida, USA. https://doi.org/10.1201/b16347

Poletto, M.; Zattera, A.J.; Forte, M.M.C.; Santana, R.M.C. 2012a. Thermal decomposition of wood: Influence of wood components and cellulose crystallite size. *Bioresour Technol* 109: 148-153. https://doi.org/10.1016/j.biortech.2011.11.122

Poletto, M.; Zattera, A.J.; Santana, R.M.C. 2012b. Structural differences between wood species: Evidence from chemical composition, FTIR spectroscopy, and thermogravimetric analysis. *J Appl Polym Sci* 126:336-343. https://doi.org/10.1002/app.36991

Poletto, M. 2016. Thermal degradation and morphological aspects of four wood species used in lumber industry. *Rev Árvore* 40(5): 941-948. http:// doi.org/10.1590/0100-67622016000500018

Properzi, M.; Leban, J.M.; Pizzi, A.; Wieland, S.; Pichelin, F.; Lehmann, M. 2005. Influence of grain direction in vibrational wood welding. *Holzforschung* 59(1): 23-27. http://doi.org/10.1515/HF.2005.004

Rodriguez, G. 2010. Soudage du bois par rotation. M.Sc. Dissertation, University of Laval. Québec, Canada. (In French)

Rowell, R.M. 2005. *Handbook of wood chemistry and wood composites*. CRC Press, Boca Raton, USA. https://doi.org/10.1201/9780203492437

Schneid, E.; Moraes, P.D. 2016. União de peças de madeira por meio da técnica de soldagem por fricção rotacional. In: Proceedings of the XV EBRAMEM – Encontro Brasileiro em Madeiras e em Estruturas de Madeira, Curitiba, Brazil. (In Portuguese)

Segal, L.C.; Creely, J.J.; Martin, A.E.J.; Conrad, C.M. 1959. An empirical method for estimating the degree of crystallinity of native cellulose using the X-ray diffractometer. *Text Res J* 29(10): 786–794. https://doi.org/10.1177/004051755902901003

Slopiecka, K.; Bartocci, P.; Fantozzi, F. 2012. Thermogravimetric analysis and kinetic study of poplar wood pyrolysis. *Appl Energy* 97: 491-497. http://doi.org/10.1016/j.apenergy.2011.12.056

Smid, P. 2003. *CNC Programing Handbook*. Industrial Press Inc, New York, USA.

Sotayo, A.; Bradley, D.; Bather, M.; Sareh, P.; Oudjene, M.; El-Houjeyri, I.; Harte, A.M.; Mehra, S.; *et al.* 2020. Review of state of the art of dowel laminated timber members and densified wood materials as sustainable engineered wood products for construction and building applications. *Dev Built Environ* 1: 100004. https://doi.org/10.1016/j.dibe.2019.100004

Stamm, B.; Windeisen, E.; Natterer, J.; Wegener, G. 2006. Chemical investigations on the thermal behaviour of wood during. *Wood Sci Technol* 40: 615-627. http://doi.org/10.1007%2Fs00226-006-0097-2

Strezov, V.; Moghtaderi, B.; Lucas, J.A. 2003. Thermal study of decomposition of selected biomass samples. *J Therm Anal Calorim* 72: 1041-1048. https://doi.org/10.1023/A:1025003306775

Sun, Y.; Royer, M.; Diouf, P.N.; Stevanovic, T. 2010. Chemical changes induced by high-speed rotation welding of wood - application to two Canadian hardwood species. *J Adhes Sci Technol* 24(8-10): 1383-1400. https://doi.org/10.1163/016942410X500990

Tsujiyama, S.; Miyamori, A. 2000. Assignment of DSC thermograms of wood and its components. *Thermochim Acta* 351(1-2): 177-181. https://doi.org/10.1016/S0040-6031(00)00429-9

Vaziri, M.; Sandberg, D. 2021. Welding of thermally modified wood and thermal modification of the welded wood: effects on the shear strength under climatic conditions. *BioResources* 16(2): 3224-3234. https://doi.org/10.15376/biores.16.2.3224-3234

Viana, A.C.C.V.; Moraes, P.D.; Weingaertner, W.L.; Zaniboni, P.N.; Prando, T. 2021. Soldagem das madeiras de pinus e de itaúba por fricção rotativa. *Rev Principia* 57: 63-75. https://doi.org/10.18265/1517-0306a2021id5809 (In Portuguese).

Viana, A.C.C.V.; Ebersbach, F.G.; Moraes, P.D.; Weingaertner, W.L. 2022a. Influence of pre-drilling hole and feed rate on welded surface strength of pine-itauba joints. *Case Stud Constr Mater* 17. https://doi.org/10.1016/j.cscm.2022.e01473

Viana, A.C.C.V.; Moraes, P.D.; Weingaertner, W.L. 2022b. União de peças de pinus a partir da soldagem de cavilhas de itaúba por fricção rotativa. In: *4º* CBLCMS – Congresso Luso-Brasileiro de Materiais de Construção Sustentáveis, Salvador, Brazil. (In Portuguese)

Wulfhorst, H.; Duwe, A.M.; Merseburg, J.; Tippkötter, N. 2016. Compositional analysis of pretreated (beech) wood using differential scanning calorimetry and multivariate data analysis. *Tetrahedron* 72(46): 7329-7334. https://doi.org/10.1016/j.tet.2016.04.029

Yang, H.; Yan, R.; Chen, H.; Lee, D.H.; Zheng, C. 2007. Characteristics of hemicellulose, cellulose and lignin pyrolysis. *Fuel* 86(12-13): 1781-1788. https://doi.org/10.1016/j.fuel.2006.12.013

Yin, W.; Lu, H.; Zheng, Y.; Tian Y. 2022. Tribological properties of the rotary friction welding of wood. *Tribol Int* 167. https://doi.org/10.1016/j.triboint.2021.107396

Zhang, J.; Gao, Y.; Zhang, J.; Zhu, X. 2018. Influence of pretreated wood dowel with $CuCl_2$ on temperature distribution of wood dowel rotation welding. *J Wood Sci* 64: 209-219. https://doi.org/10.1007/s10086-017-1693-5

Zhu, X.; Gao, Y.; Yi, S.; Ni, C.; Zhang, J.; Luo, X. 2017a. Mechanics and pyrolysis analyses of rotation welding with pretreated wood dowels. *J Wood Sci* 63: 216-224. https://doi.org/10.1007/s10086-017-1617-4

Zhu, X.; Yi, S.; Gao, Y.; Zhao Y.; Qiu, Y. 2017b. Mechanical evaluation and XRD/TG investigation on the properties of wooden dowel welding. *BioResources* 12(2): 3396-3412. 10.15376/BIORES.12.2.3396-3412

Zhu, X.; Xue, Y.; Zhang, S.; Shen, J.; Yi, S.; Gao, Y. 2018. Mechanics and crystallinity/thermogravimetric investigation into the influence of the welding time and $CuCl_2$ on wood dowel welding. *BioResources* 13(1): 1329-1347. http://doi.org/10.15376/biores.13.1.1329-1347

Zor, M.; Görgün, H.V.; Vaziri, M. 2021. X-ışını Kırınımı (XRD) ve Taramalı Elektron Mikroskobu (SEM) Kullanılarak Kaynaklanan Göknar, Meşe ve Kestane Odununun Yapısal Karakterizasyonu. *J Bartin Faculty Forestry* 23(3): 871-877. https://doi.org/10.24011/barofd.989542 (In Turkish)